Green and facile synthesis of zinc oxide nanoparticles for enhanced photocatalytic organic pollutant degradation

C. Mallikarjunaswamy[1],* ⬥, P. Parameswara[2], S. Pramila[1], G. Nagaraju[3], H. N. Deepakumari[4], and V. Lakshmi Ranganatha[5],*

[1] Postgraduate Department of Chemistry, JSS College of Arts, Commerce and Science and JSS Research Centre (A Recognized Research Centre of University of Mysore), Mysuru, Karnataka 570025, India

[2] Department of Physics, The National Institute of Engineering, Manandavadi Road, Mysuru, Karnataka 570008, India

[3] Energy Materials Research Laboratory, Department of Chemistry, Siddaganga Institute of Technology, Tumakuru, Karnataka 572103, India

[4] Department of Chemistry, Bharathi College, Bharathinagara, Mandya, Karnataka 571422, India

[5] Department of Chemistry, The National Institute of Engineering, Manandavadi Road, Mysuru, Karnataka 570008, India

ABSTRACT

ZnO nanoparticles show great potential for photodegradation applications due to their excellent physical and chemical properties. Finding a greener approach to producing nanoparticles is of the utmost importance for multidimensional application purposes. In the present study, the ZnO nanoparticles were synthesized by a simple combustion method at 400 °C, using jackfruit extract. X-ray diffraction (XRD) pattern revealed a crystalline structure of the nanoparticles. Scanning electron microscope (SEM), Raman spectroscopy, BET surface area were used to further characterize the synthesized nanoparticles. Further, it has been used as a photocatalyst for the degradation of one of the organic pollutant methylene blue dye. In general, the method employed here is a greener approach to synthesize ZnO nanoparticles with good photocatalytic activity.

1 Introduction

Starting from the development of TiO_2 by Fujishima and Honda in the year 1972 [1] has gradually been increasing in the application of nanomaterials for environmental cleanup. In the present advanced science and engineering fields, nanotechnology is one of the dynamic fields. Nanotechnology mainly deals with the physical and chemical properties of materials having a size less than 100 nm and it mainly depends on the morphology, size distribution, and atomic and molecular combinations of the materials. Till today researchers have been synthesized modified TiO_2 [2], ZnO [3–5], ZrP_2O_7 [6], ZrO_2 [7], SnO_2 [8], CuO [9], NiO [10], $BiVO_4$ [11], Bi_2WO_6 [12] $ZnFe_2O_4$ [13], BiOCl [14], $Mn_2V_2O_7$ [15], ZrO_2 [7, 16],

etc. Among all the nanomaterials ZnO has become one the most extensively investigated due to its wider application in the field of environmental cleanup, solar energy conversions [17], photocatalysts, opto-electronics and excellent photoelectrochemical properties. Consequently, many researchers have synthesized metal-loaded and nonmetal-loaded ZnO [18] nanomaterials such as Ag/ZnO [19], rGO/ZnO [20], etc. While ZnO is the most stable semiconductor material used to solve environmental problems.

Due to industrialization and urbanization, clean water availability is very less, this leads many researchers to think about the best way to clean up the water. Even now many conventional methods have been used such as adsorption, bio-flocculation, filtration, etc. for cleaning water. But, all the methods are expensive and lead to secondary pollutants. Therefore, nanotechnology plays a vital role in the crackdown of environmental pollutants and also helps for the generation of cleaner energy by the water-splitting method. In this context, we planned to synthesize ZnO nanoparticles by using an environmentally benign green protocol. Many methods such as sonochemical method, co-precipitation method, hydrothermal method, combustion method using chemicals like fuels, biosynthesis method, sol–gel method, but nowadays, green synthesis of nanomaterials has led to the development of an eco-friendly approach. In recent years many researchers have synthesized nanomaterials using plant extracts [21–25] as a fuel in combustion method synthesis, these extracts not only act as reducing agents but also act as capping agents and reduce the size of the nanoparticles. The plant sources are the first choice of research aiming for the synthesis of nanoparticles because of abundant biomass, molecular repertoires, and species diversity, the fact is that plants produce a wide variety of primary and secondary metabolites [26–29]. The metabolites are amino acids [30], polypeptides [31], enzymes [32], polysaccharides [33], tannins [34], heterocyclic compounds [35], flavonoids [36] and, phenolic compounds [37] etc., are responsible for reduction of metals. Indeed different plants may produce different characteristic nanoparticles, because of different phytochemical profiles with different concentrations.

A large number of medicinal plants like *Alternanthera dentate*, *Vitex negundo*, *Brassica rapa*, *Ocium sanctum*, *Acorus calamus*, *Solanum xanthcarpum*, *Andrographis paniculata* have been used by researchers for the synthesis of different metal oxide nanoparticles. In this present study, we have used a low-cost facile solution combustion method for the preparation of zinc oxide nanoparticles using aqueous tender jackfruit extract. The synthesized nanoparticles are tested for photocatalytic activity using methylene blue dye as a model organic dye and it is one of the main wastes that come from the textile industries. This organic dye will cause a serious threat to the environment as well as human health.

2 Materials and methods

2.1 Preparation of extract (fuel)

The jack fruit extract was prepared by taking fresh tender jack fruit and dried in shadow for 15 days. The dried fruit was ground mechanically using a mixer grinder. The powder was subjected to soxhlet apparatus at 80–90 °C for 48 h or 15 cycles. Then, the extract was filtered using ordinary filter paper and was stored in the refrigerator for further use.

2.2 The preparation of ZnO nanoparticles

The as-prepared extract was used to prepare ZnO nanoparticles, the 0.1 M zinc nitrate hexahydrate was used as a source of Zn. A series of crucibles were taken and 1, 2, and 3 ml of extract (labeled as ZnO/1, ZnO/2, and ZnO/3) were transferred to them to optimize the volume of fuel. 0.1 M source was added to each crucible and stirred for about 15 min on a hot plate to get a homogeneous semisolid liquid. Then, the crucibles were kept inside a 400 °C pre-heated muffle furnace. The smoldering type reaction took place with the liberation of gases within 15 min. The obtained product was then subjected to calcination to remove all the impurities present. The synthesized nanomaterials were used to study photodegradation using methylene blue organic dye.

2.3 Characterization

The crystallinity of the material was confirmed by using Rigaku smart lab diffractometer (Cu-Kα, 1.5418). The surface morphology is very important for nanomaterials, so this was elucidated using the TESCAN Vega 3LMU scanning electron microscope and also elemental composition and purity of the

material were confirmed. The Quanta chrome Nova-1000 surface analyzer was used to confirm the pore size and surface area under Liq. N_2 temperature. The photodegradation performance and optical properties were studied using Agilent Cary 60 UV–Vis spectrophotometer. The Raman measurements were recorded using Horiba xplora plus Raman spectroscope.

2.4 Photodegradation study of ZnO nanoparticles

The photocatalytic activity of ZnO nanoparticles was carried out in an annular type photoreactor. A catalytic load of 30 mg in 100 ml of 5 ppm methylene blue dye was prepared and pH was adjusted by adding 0.5 M NaOH and 0.5 M HCl. The resultant solution was placed in the photoreactor and an air purge was done to stop the settling of nanoparticles at the bottom. The high-pressure mercury lamp (250 W, 365 nm) was fitted inside a quartz chamber surrounded by a water-cooled condenser, the solution was 12 cm away from the UV source, and the sample was kept in dark condition to attain adsorption–desorption equilibrium. The degradation of methylene blue dye was measured by removal of solution after intervals of time. The maximum absorption of methylene blue dye was 664 nm (due to chromosphere) and 292 nm (due to the aromatic rings). (C_f and C_i are final and initial concentrations of methylene blue dye, respectively)

$$\text{Degradation efficiency} = \frac{C_i - C_f}{C_i} \times 100 \tag{1}$$

3 Results and discussion

3.1 Characterization

3.1.1 XRD studies

Figure 1 shows the XRD pattern of ZnO nanoparticles prepared by using jack fruit extract as a fuel with different concentrations of 1 ml, 2 ml, and 3 ml. The XRD patterns confirm the structural composition and crystalline nature of ZnO nanoparticles. All the peaks (100), (002), (101), (102), (110), (103), and (112) well match with hexagonal zincite (Wurtzite) structure. Further, no additional peaks observed in the

spectrum confirm the purity of the material. The average crystalline size was estimated using Debye–Scherrer's equation.

$$D = \frac{0.89\lambda}{\beta \cos \theta}$$

where D is the crystallite size, λ is the X-ray wavelength, β is the full width at the half maximum and θ is the diffraction angle. The crystallite size was found to be 15 nm.

3.2 Morphological analysis

The surface morphology and elemental composition of ZnO nanoparticles were confirmed by scanning electron microscope and energy-dispersive X-ray analysis (Figs. 2 and 3). The ZnO nanoparticles are agglomerated during the combustion process and form a small capsule-like structure. The chemical composition of the ZnO is 51.23% zinc and 48.77% oxygen.

3.3 BET surface area analysis

The surface properties like pore size, pore-volume, and surface area of nanomaterials play an important role in their properties. Figure 4 shows the N_2 adsorption/desorption isotherm and pore size distribution of ZnO nanomaterials and it explains the Langmuir hysteresis curve of type IV isotherm and this type of curve depends on the shape of the pore in the particular sample. The surface area of the ZnO/1,
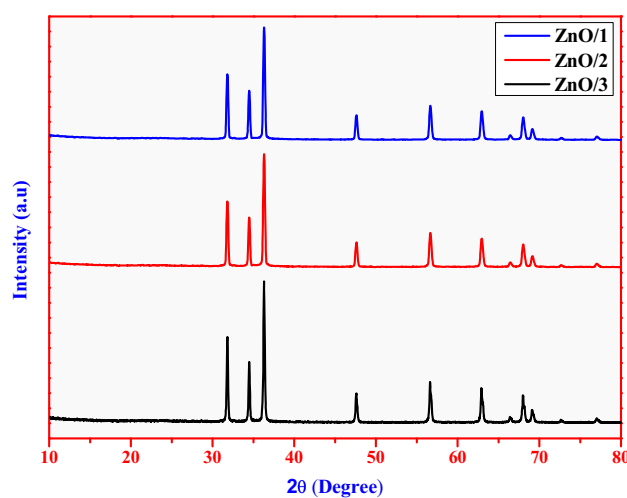

Fig. 1 Diffraction patterns of as-prepared ZnO nanoparticles

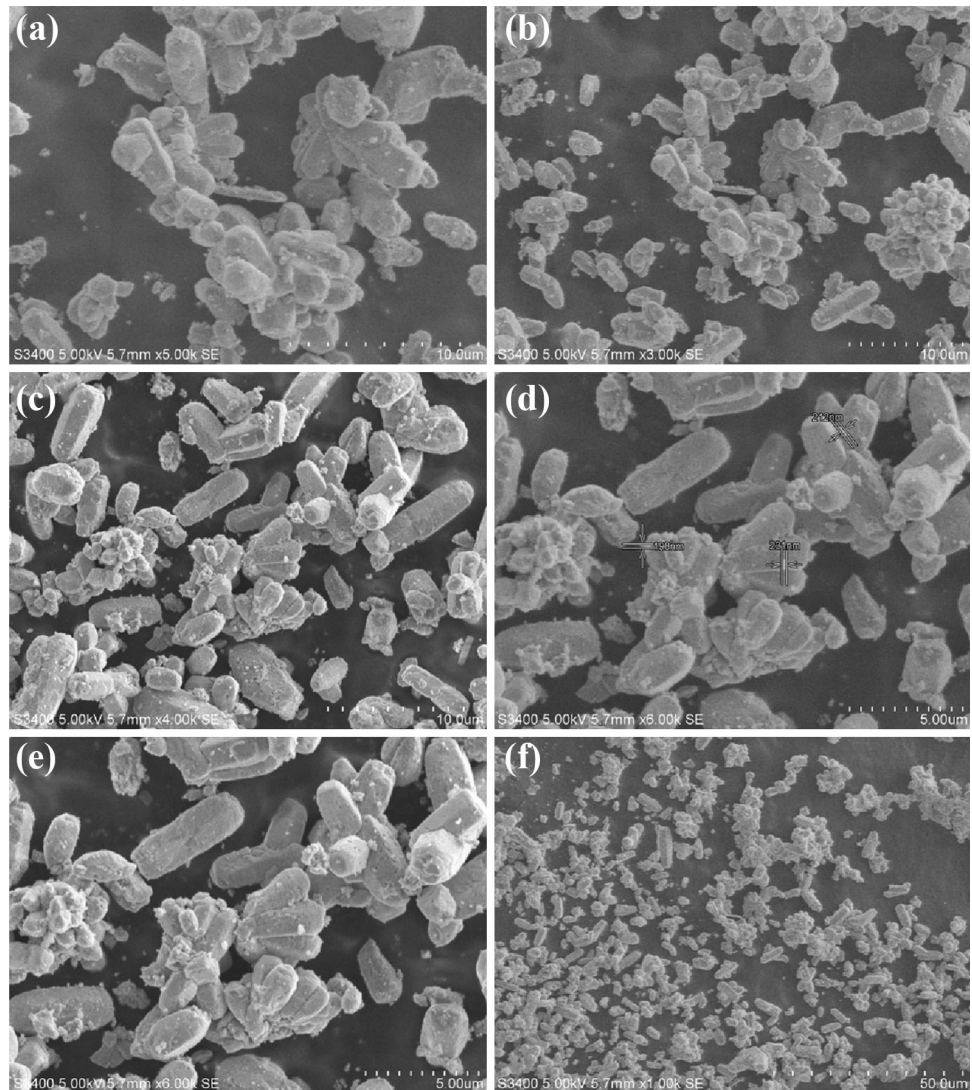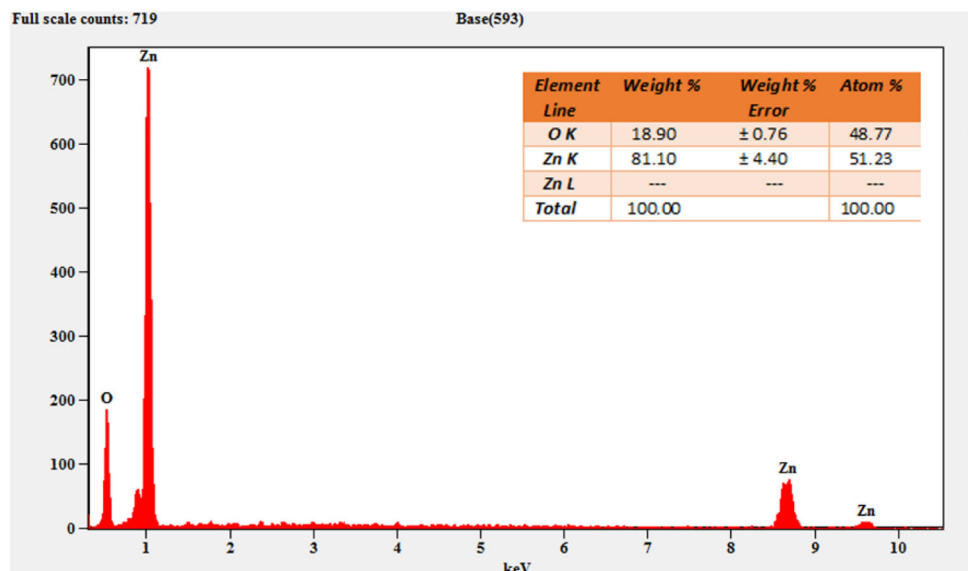**Fig. 2** SEM images of as-prepared ZnO nanoparticles

Fig. 3 EDS spectrum of as-prepared ZnO nanoparticles

ZnO/2, and ZnO/3 was 20.8 m² g⁻¹, 25.3 m² g⁻¹, and 22.1 m² g⁻¹, respectively.

3.4 Raman scattering

Raman scattering is used to study the crystalline nature of the nanomaterials and also used to find the defects in the synthesized ZnO nanomaterials. Figure 5 shows the Raman scattering spectrum of ZnO nanoparticles synthesized using jack fruit extract as a fuel. The prominent peaks at 336 cm⁻¹ and 442 cm⁻¹ correlate to the E_{2H}–E_{2L}, and A_1(TO) fundamental phonon modes of ZnO hexagonal structure, respectively. The strong peak at 442 cm⁻¹ E2 modes corresponds to Wurtzite structured ZnO nanomaterials. And another well-resolved peak at 583 cm⁻¹ correlates to E2 due to resonance and multiphonon process and is related to oxygen deficiency.

3.5 UV–Visible studies

The optical properties of the prepared ZnO nanomaterials were studied using UV–Visible studies, this is one of the effective tools to find the primary existence of metal oxide nanoparticles in an aqueous medium. This is the unique technique used to check the bandgap energy of the material, nanoparticles have a particular absorption wavelength due to their characteristic optical property. Figure 6 shows that the strong absorption peak at 377 nm is due to the absorption of the host lattice, it suggesting that ZnO nanoparticles can be excited by UV light. Thus by using this absorption wavelength, the bandgap (E_g)
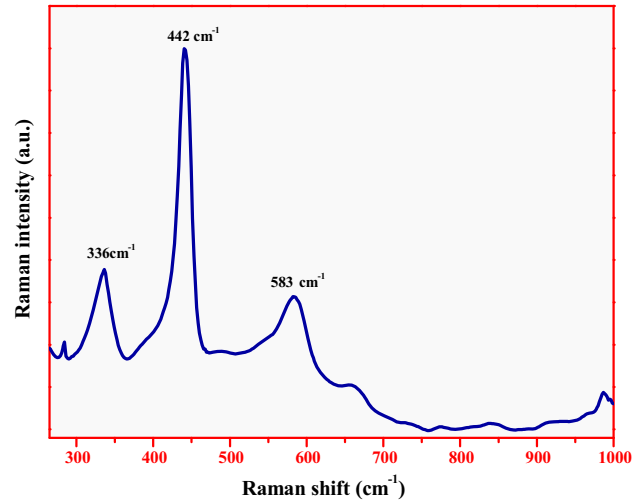
Fig. 5 Raman plot of ZnO nanoparticles

energy of ZnO Nanoparticles can be obtained from the absorbed wavelength value using the energy equation [38].

$$E = \frac{hc}{\lambda} \tag{2}$$

where Energy (E) = Band gap, h is Planks constant (6.626×10^{-34} Joules s⁻¹), C is velocity of light (2.99×10^8 m/s), and λ is wavelength that is absorption peak. From Fig. 6, absorption band appeared at 377 nm and the band gap value is calculated form equation which was found to be 3.15 eV and it was also confirmed by UV-DRS spectrum. This wide band gap is probably due to small particle size [39].
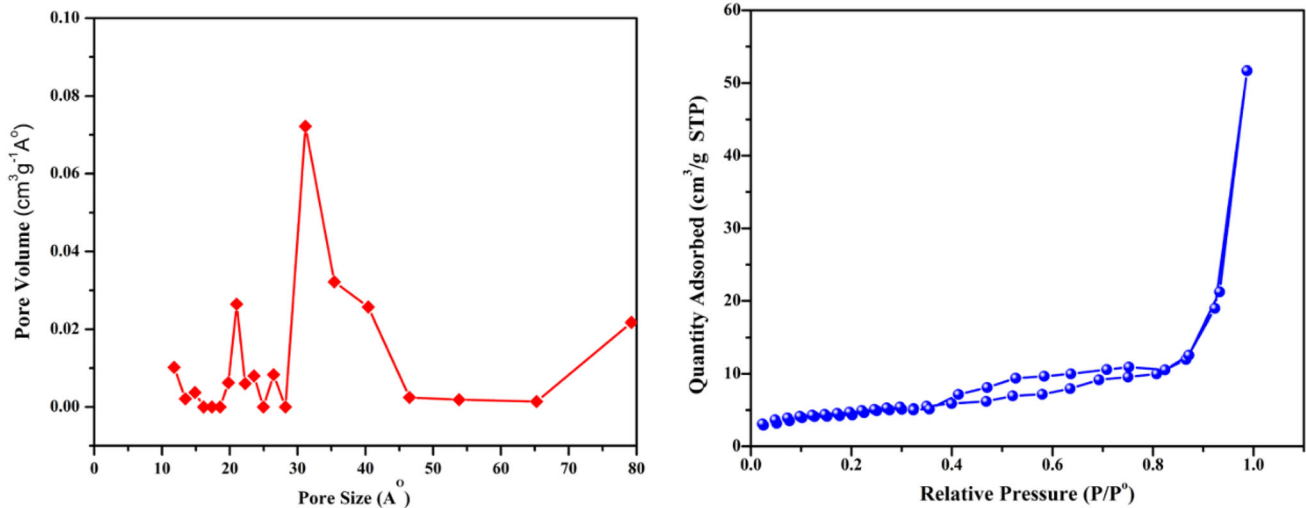
Fig. 4 Nitrogen adsorption/desorption isotherm and pore size distribution of ZnO nanoparticles
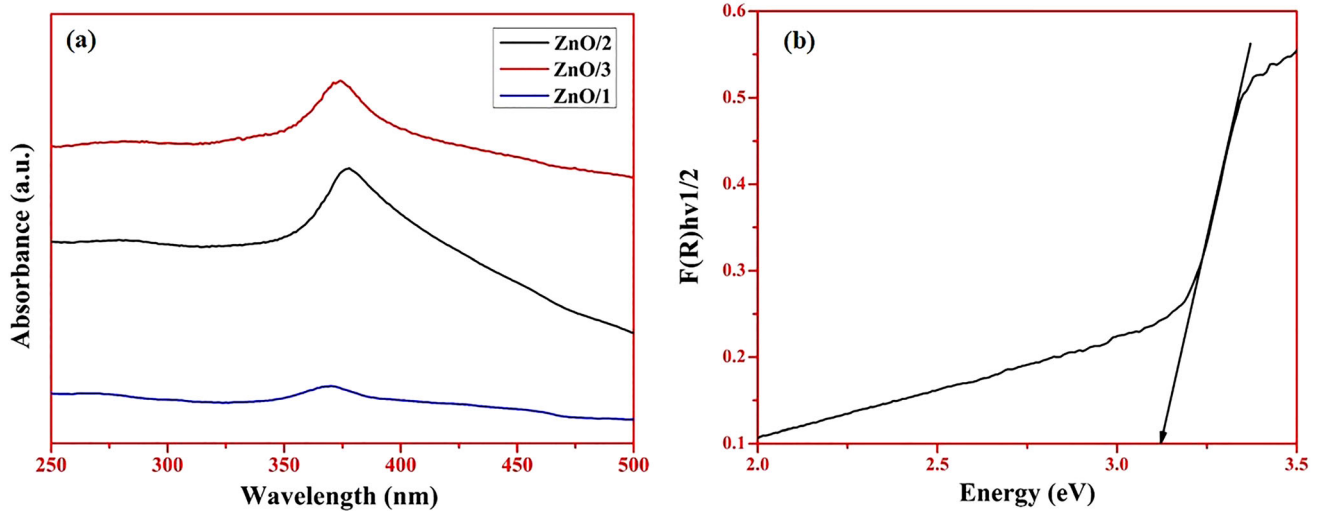
Fig. 6 **a** UV–Visible and **b** UV-DRS spectrum of ZnO nanoparticles

4 Photocatalytic activity of ZnO nanoparticles

The synthesized zinc oxide nanoparticles by varying fuel volumes were subjected to perform photodegradation of Methylene blue dye under UV light radiation. The photodegradation efficiency of methylene blue dye carried out by ZnO nanoparticles were illustrated in the Fig. 7. It reveals that the fuel affects the photocatalytic activity of zinc oxide nanoparticles because activity mainly depends on the surface area of the nanoparticles. The photocatalytic efficiency is 85.9%, 97.9% and 78.4% within 60 min for the sample prepared using 1 ml, 2 ml, and 3 ml fuel, respectively. The photochemical reaction of ZnO/2 material is fairly more when compared to ZnO/1 and ZnO/3. The order of the photodegradation efficiency was found to be ZnO/2 > ZnO/1 > ZnO/3 after 60 min of UV light irradiation and it may be due to optical properties, crystallite size, and surface area of the ZnO nanoparticles. The fuel volume modifies the oxygen vacancies, these oxygen vacancies trap photo-excited electrons present in the conduction band which gives more dye degradation efficiency. The degradation completes 98% within 60 min indicating the low recombination rate of electrons. The calcination temperature of 400 °C also influences surface morphology which enhances photocatalytic activity. Further, the photocatalytic activity of the ZnO nanoparticles prepared without fuel was > 50% degradation efficiency it may be due
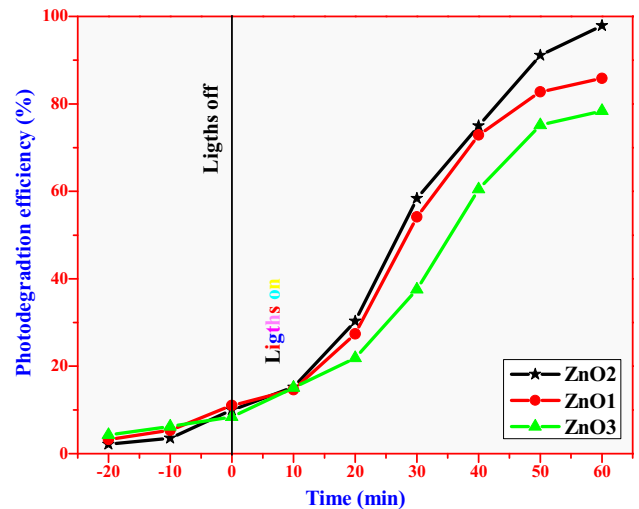

Fig. 7 Photodegradation efficiency of different ZnO nanoparticles

to organic molecules present in the fuel controlling the growth of nanoparticles.

4.1 Effect of catalyst load on photocatalytic activity

The aim of optimization of catalyst load is a crucial phase in the photodegradation process. Catalyst affects the photodegradation of methylene blue dye in the photochemical reaction. Figure 8 indicates the ZnO nanoparticles prepared using different volumes and photodegradation of methylene blue under UV irradiation. The photodegradation efficiency increased from 70 to 98% as the amount varied different 10 to 20 mg, respectively. This increase in

photodegradation is due to the larger surface area of the ZnO/2 nanoparticle. This larger surface area influences the creation of active sites and leads to the generation of more hydroxyl radicals. The excess nanoparticles (30 mg) shielded the penetration of light to the surface of the photocatalyst. Thus, the generation of hydroxyl radicals reduces and there will be a decrease in photodegradation of methylene blue dye.

4.2 Effect of pH on methylene blue dye degradation

The pH very important parameter to study in photodegradation activity (Fig. 9). The effect of pH was studied from pH 4 to 11 to check the optimum pH for the photodegradation of methylene blue dye. From the Fig. 10 we can conclude that there will be gradual increasing degradation of methylene blue from 3 to 7 and maximum degradation recorded at pH 11. Above this pH the degradation decreases, which can be explained on the basis of zero potential charge. For ZnO the zero potential charge was found to 9.0 ± 0.3, and above this value the surface is negatively charged due to adsorbed OH^- ions. The presence of many OH^- ions on the surface of catalyst causes less production of $OH\cdot$ radicals, which act as primary oxidizing agents and which are accountable for the degradation of methylene blue dye.
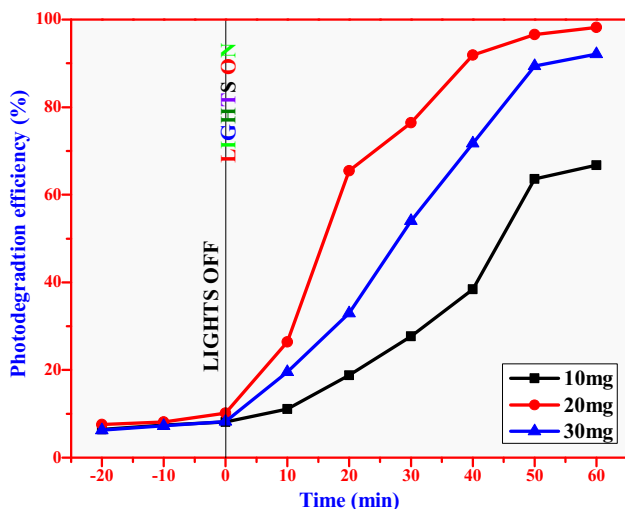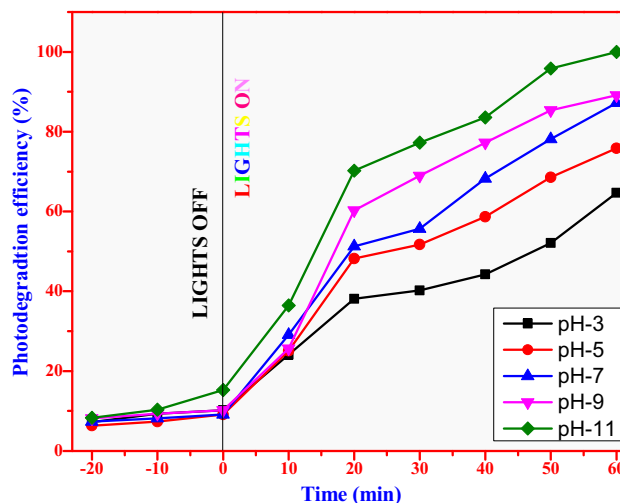

Fig. 9 Effect of pH on photocatalytic degradation of methylene blue dye

4.3 Effect of concentration of methylene blue dye

The concentration of dye varied from 5 to 20 ppm with a constant 20 mg catalyst load as indicated in Fig. 10. The efficiency of degradation is more up to 10 ppm and after this, there is a decreased efficiency. Because the light does not penetrate so a decrease in the photodegradation efficiency.

4.4 Reproducibility of photocatalyst

The repercussion of the photocatalytic system very much depends on the recyclability and regeneration of the photocatalyst without decreasing the efficiency

Fig. 8 Effect of catalyst load on Photocatalytic degradation of methylene blue dye
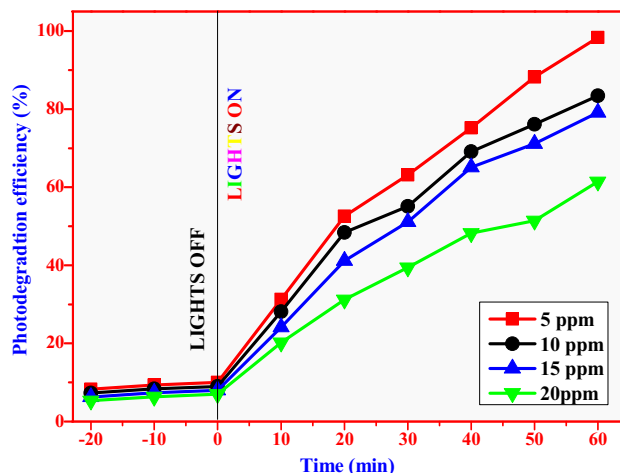

Fig. 10 Effect of dye concentration on Photocatalytic degradation of methylene blue dye

of the photodegradation. Recyclability was conducted by using 100 mg of ZnO nanoparticles under UV irradiation. After each cycle, the nanocatalyst was washed repeatedly with distilled water and dried in an oven at 110 °C for 2 h. Up to five cycles, the recovered catalyst show almost the same efficiency as that of the freshly used catalyst. After the sixth cycle, there is a slight reduction in efficiency of about 6% (Fig. 11). Nevertheless, the difference in degradation effect is very low and ZnO nanoparticles possess good stability and recycling ability during the photochemical reaction.

4.5 Detection of OH• radicals

The photocatalytic degradation mainly depends on the generation of hydroxyl radicals, these are the reactive oxygen species responsible for the degradation of methylene blue dye. The generation of these radicals can be measured by the photoluminescence technique using coumarin as a probe molecule. In this technique, hydroxyl radical reacts with coumarin to form 7-hydroxy coumarin which is highly fluorescent and has an excitation wavelength of 452 nm. In this process, 10^{-3} molar coumarin was prepared. To the above-prepared solution 50 mg of coumarin was added (Fig. 12). Initially, the mixture was allowed to stand for 30 min for the adsorption–desorption equilibrium process, after attainment UV light was irradiated. For every 10 min interval, 2 ml aliquots were withdrawn from the reaction mixture
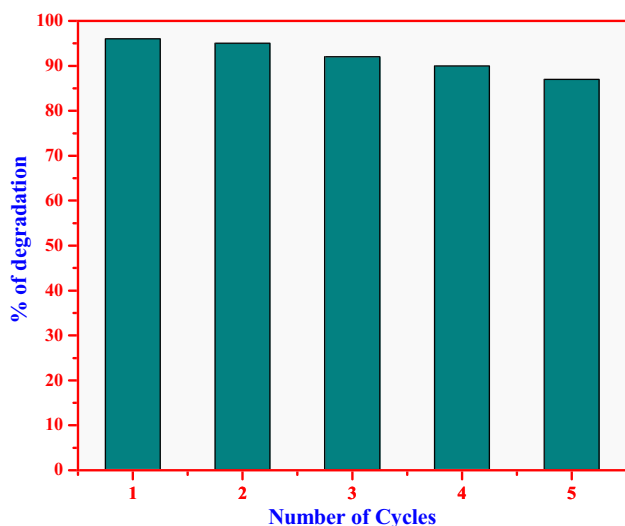
and subjected to a photo luminescent spectrophotometer. Fig. clearly indicates the increase in the intensity of the peak at 457 as the concentration of hydroxyl radicals increases. This process confirms the reactive oxygen species importance in photocatalytic degradation of methylene blue organic dye.

4.6 Mechanism of photodegradation

At the surface of the photocatalyst, the photochemical (redox) reaction is initiated when light irradiation starts. The potential values of the conduction band and valance band were calculated using the following formulae:

$$E_{CB} = \chi - E_0 - \frac{1}{2}E_g$$

$$E_{VB} = E_{CB} + E_g$$

E_{VB} and E_{CB} are the valance band edge potential and conduction band edge potential, respectively, and E_g is the bandgap of the semiconductor which is 3.12. When UV light falls on the VB the electrons absorb photons and are excited to CB leaving holes in the VB. The generated e^- and h^+ may react with other molecules or they may either recombine. If the recombination is more, then there will be a decrease in photodegradation efficiency. The oxygen vacancies can trap the electrons from the CB so there is a decrease in recombination of electron–hole. This will increase the photocatalytic activity of ZnO nanoparticles. The h^+ in the VB will react with hydroxyl ions generated from the water and accumulate on the
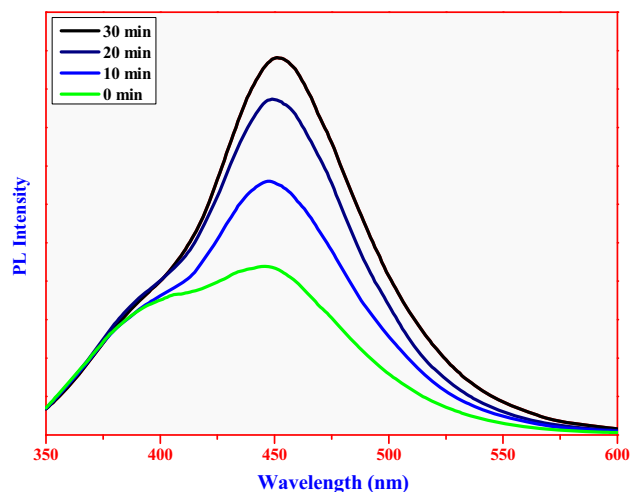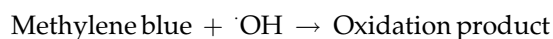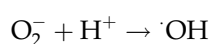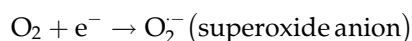
Fig. 11 Recycling of 100 mg catalyst for the degradation of 100 ml of 5 ppm methylene blue dye
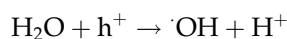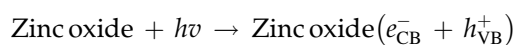
Fig. 12 Photoluminescence (PL) spectrum for detection of hydroxyl radicals

surface of the catalyst to form highly reactive OH radicals. While the e^- is absorbed by O_2 to form O_2. The generated OH radicals are strong oxidizing agents and attack MB dye to convert MB to non-toxic products, thereby decreasing the concentration of dye (Fig. 13).

The probable reaction mechanism of degradation of methylene blue is as follows;

$$Zinc\,oxide + hv \rightarrow Zinc\,oxide(e_{CB}^- + h_{VB}^+)$$

$$H_2O + h^+ \rightarrow {}^{\cdot}OH + H^+$$

$$OH^- + h^+ \rightarrow {}^{\cdot}OH\,(hydroxyl\,radical)$$

$$O_2 + e^- \rightarrow O_2^-\,(superoxide\,anion)$$

$$O_2^- + H^+ \rightarrow {}^{\cdot}OH$$

$$Methylene\,blue + {}^{\cdot}OH \rightarrow Oxidation\,product$$

$$Methylene\,blue + h^+ \rightarrow Oxidation\,of\,methylene\,blue$$

4.7 Total organic carbon content test (TOC)

Total organic carbon content test is the measure of the level of organic molecules/impurities in purified water sample. It has become an important parameter used to monitor overall levels of organic compounds present. In this study, we have used this analytical technique to find out the purity of water sample after and before MB dye degradation. Further, APHA 5310 22nd Edition test method was used to analyze the samples. Samples were tested before (colored sample) and after dye degradation (colorless sample) assay and we found 18 mg L^{-1} and < 2 mg L^{-1} of total organic carbon content, respectively, in the tested samples.

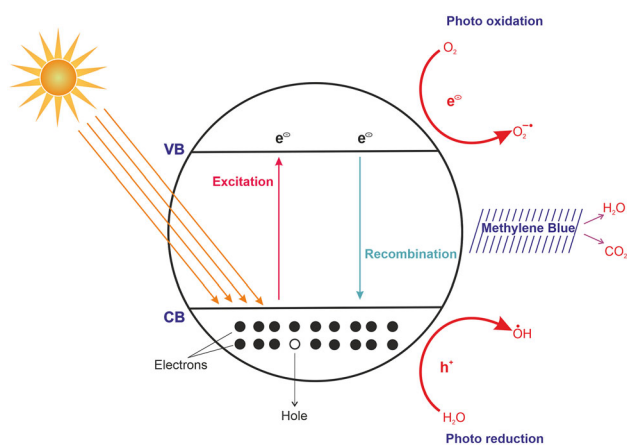### 4.8 Detection of reactive oxygen species

The different scavengers are used to study the reactive species which are involved in the degradation of methylene blue dye. These scavengers trap the reactive species (holes, superoxides, hydroxyl radicals) and reduce their production. This experiment was conducted by using ethylenediamine tetra acetic acid disodium salt (EDTA-2Na, 1 mM), $K_2Cr_2O_7$ (1 mM), tert-butyl alcohol (TBA, 1 mM) scavengers for holes (h^+), superoxide anion radical ($O_2^{\cdot-}$), and hydroxyl radical (·OH), respectively, [18] depicted in the Fig. 14. These results conveyed that degradation percentage was greatly decreases in the presence of TBA, hence, hydroxyl radicals are mainly responsible for the degradation of MB dye [40].

5 Conclusion

The novel and effective jack fruit extract as fuel was used to prepare ZnO nanoparticles. The as-prepared ZnO nanoparticles were characterized by XRD which revealed the lattice parameter and hexagonal Wurtize structure. The absorption spectrum at 377 nm is assigned to be intrinsic bandgap absorption. SEM images show uniform distributed capsules/rod-shaped ZnO nanoparticles. The as-prepared nanoparticles have a band gap of 3.12 eV showing good photocatalytic activity against methylene blue organic dye. This study demonstrates the simple and cost-effective utilization of greener extracts as fuel for

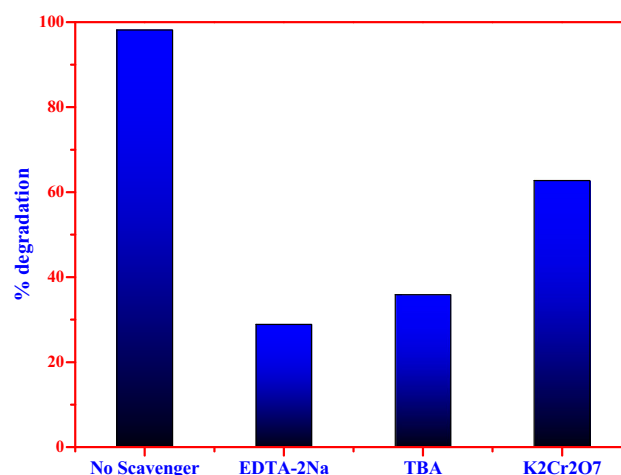Fig. 13 Diagrammatic illustration of degradation mechanism

Fig. 14 Photocatalytic activity of the ZnO nanoparticles for the degradation of MB dye with different scavengers

morphologically, structurally good, and potential ZnO photocatalyst for degradation applications.

Acknowledgements

Author contributions

All authors contributed to the study's conception and design. Material preparation, data collection, and analysis were performed by CM, SP, HND, GN, PP, and VLR. The first draft of the manuscript was written by CM and all authors commented on previous versions of the manuscript. All authors read and approved the final manuscript.

Data availability

All data generated or analyzed during this study are included in this published article.

Declarations

Conflict of interest The authors do not have any conflict of interest.

References

1. A. Fujishima, K. Honda, Electrochemical photolysis of water at a semiconductor electrode. Nature **238**, 37 (1972)
2. D. Komaraiah, E. Radha, J. Sivakumar, M.V.R. Reddy, R. Sayanna, Photoluminescence and photocatalytic activity of spin coated Ag+ doped anatase TiO_2 thin films. Opt. Mater. (Amst). **108**, 110401 (2020)
3. B.S. Surendra, M.M. Swamy, T. Shamala, S. Rao, A.S. Sowmy, C. Mallikarjuna, S. Pramila, Development of enhanced electrochemical sensor and antimicrobial studies of ZnO NPs synthesized using green plant extract. Sens. Int. **3**, 100176 (2022). https://doi.org/10.1016/j.sintl.2022.100176
4. A. Info, CO CO, (2015).
5. C. Mallikarjunaswamy, J.S. Vidya, H.N. Deepakumari, G. Nagaraju, M.A. Sangamesha, Larvicidal and antimicrobial activity of zinc oxide nanoparticles synthesized from rain tree pod aqueous extract. Mater. Today (2022). https://doi.org/10.1016/j.matpr.2022.02.422
6. H.N. Deepakumari, V.L. Ranganatha, G. Nagaraju, R. Prakruthi, C. Mallikarjunaswamy, Facile green synthesis of zirconium phosphate nanoparticles using *Aegle marmelos*: antimicrobial and photodegradation studies. Mater. Today (2022). https://doi.org/10.1016/j.matpr.2022.02.579
7. V.L. Ranganatha, G. Nagaraju, J.S. Vidya, H.N. Deepakumari, D.M. Gurudutt, Indian bael mediated eco-friendly synthesis and performance evaluation of zirconium oxide nanoparticles: an efficient anti-microbial agent. Mater. Today (2022). https://doi.org/10.1016/j.matpr.2022.02.407
8. S. You, H. Zeng, Z. Ku, X. Wang, Z. Wang, Y. Rong, Y. Zhao, X. Zheng, L. Luo, L. Li, Multifunctional polymer-regulated SnO_2 nanocrystals enhance interface contact for efficient and stable planar perovskite solar cells. Adv. Mater. **32**, 2003990 (2020)
9. T.I. Shaheen, A. Fouda, S.S. Salem, Integration of cotton fabrics with biosynthesized CuO nanoparticles for bactericidal activity in the terms of their cytotoxicity assessment. Ind. Eng. Chem. Res. **60**, 1553–1563 (2021)
10. K. Kannan, D. Radhika, M.P. Nikolova, K.K. Sadasivuni, H. Mahdizadeh, U. Verma, Structural studies of bio-mediated NiO nanoparticles for photocatalytic and antibacterial activities. Inorg. Chem. Commun. **113**, 107755 (2020)
11. C. Mallikarjunaswamy, S. Pramila, G. Nagaraju, R. Ramu, V.L. Ranganatha, Green synthesis and evaluation of antiangiogenic, photocatalytic, and electrochemical activities of $BiVO_4$ nanoparticles. J. Mater. Sci. Mater. Electron. **32**, 14028–14046 (2021)
12. C. Lu, X. Li, Q. Wu, J. Li, L. Wen, Y. Dai, B. Huang, B. Li, Z. Lou, Constructing surface plasmon resonance on Bi_2WO_6 to boost high-selective CO_2 reduction for methane. ACS Nano **15**, 3529–3539 (2021)
13. V.L. Ranganatha, S. Pramila, G. Nagaraju, B.S. Surendra, C. Mallikarjunaswamy, Cost-effective and green approach for the synthesis of zinc ferrite nanoparticles using *Aegle marmelos* extract as a fuel: catalytic, electrochemical, and microbial applications. J. Mater. Sci. Mater. Electron. **31**, 1–18 (2020)
14. D. Zhang, C. Su, S. Yao, H. Li, X. Pu, Y. Geng, Facile in situ chemical transformation synthesis, boosted charge separation, and increased photocatalytic activity of $BiPO_4$/BiOCl pn heterojunction photocatalysts under simulated sunlight irradiation. J. Phys. Chem. Solids **147**, 109630 (2020)
15. C. Mallikarjunaswamy, Enhanced photocatalytic, electrochemical and antimicrobial activities of a -$Mn_2V_2O_7$ nanopebbles. J. Mater. Sci. Mater. Electron. **33**, 617–634 (2022). https://doi.org/10.1007/s10854-021-07331-1

16. A. Tsoukalou, P.M. Abdala, A. Armutlulu, E. Willinger, A. Fedorov, C.R. Müller, Operando X-ray absorption spectroscopy identifies a monoclinic ZrO_2: in solid solution as the active phase for the hydrogenation of CO_2 to methanol. ACS Catal. **10**, 10060–10067 (2020)

17. K. Rajeshwar, R. McConnell, K. Harrison, S. Licht, *Renewable Energy and the Hydrogen Economy* (Springer, New York, 2008), pp.1–18

18. C. Mallikarjunaswamy, V.L. Ranganatha, R. Ramu, G. Nagaraju, Facile microwave-assisted green synthesis of ZnO nanoparticles: application to photodegradation, antibacterial and antioxidant. J. Mater. Sci. Mater. Electron. **31**, 1–18 (2020)

19. P. Panchal, D.R. Paul, A. Sharma, P. Choudhary, P. Meena, S.P. Nehra, Biogenic mediated Ag/ZnO nanocomposites for photocatalytic and antibacterial activities towards disinfection of water. J. Colloid Interface Sci. **563**, 370–380 (2020)

20. S. Elbasuney, G.S. El-Sayyad, H. Tantawy, A.H. Hashem, Promising antimicrobial and antibiofilm activities of reduced graphene oxide-metal oxide (RGO-NiO, RGO-AgO, and RGO-ZnO) nanocomposites. RSC Adv. **11**, 25961–25975 (2021)

21. T. Gur, I. Meydan, H. Seckin, M. Bekmezci, F. Sen, Green synthesis, characterization and bioactivity of biogenic zinc oxide nanoparticles. Environ. Res. **204**, 111897 (2022)

22. F. Khan, A. Shahid, H. Zhu, N. Wang, M.R. Javed, N. Ahmad, J. Xu, M.A. Alam, M.A. Mehmood, Prospects of algae-based green synthesis of nanoparticles for environmental applications. Chemosphere **293**, 133571 (2022)

23. Z. Guan, S. Ying, P.C. Ofoegbu, P. Clubb, C. Rico, F. He, J. Hong, Green synthesis of nanoparticles: current developments and limitations. Environ. Technol. Innov. **26**, 102336 (2022)

24. C. Mallikarjunaswamy, H.N. Deepakumari, G. Nagaraju, A. Khosla, C. Manjunatha, Eco-friendly green synthesis, characterizations, and antimicrobial activities of nickel oxide nanoparticles. ECS Trans. **107**, 16303 (2022)

25. R.S. Varma, Green-synthesized nanocatalysts and nanomaterials for water treatment: current challenges and future perspectives. J. Hazard. Mater. **401**, 123401 (2020). https://doi.org/10.1016/j.jhazmat.2020.123401

26. C.P. Devatha, A.K. Thalla, *Green Synthesis of Nanomaterials* (Elsevier, Amsterdam, 2018), pp.169–184

27. D.L. Villaseñor-Basulto, M.-M. Pedavoah, E.R. Bandala, *Plant Materials for the Synthesis of Nanomaterials: Greener Sources* (Springer, Cham, 2019), pp.105–121

28. D. Thangadurai, J. Naik, J. Sangeetha, A.R.M.S. Al-Tawaha, C.O. Adetunji, S. Islam, M. David, A.K. Shettar, J.B. Adetunji, *Nanomaterials from Agrowastes: Past, Present, and the Future* (Springer, Cham, 2021), pp.471–487

29. S. Fahimirad, F. Ajalloueian, M. Ghorbanpour, Synthesis and therapeutic potential of silver nanomaterials derived from plant extracts. Ecotoxicol. Environ. Saf. **168**, 260–278 (2019)

30. Y. Shao, Y. Jin, S. Dong, Synthesis of gold nanoplates by aspartate reduction of gold chloride. Chem. Commun. **9**, 1104–1105 (2004)

31. Y.N. Tan, J.Y. Lee, D.I.C. Wang, Uncovering the design rules for peptide synthesis of metal nanoparticles. J. Am. Chem. Soc. **132**, 5677–5686 (2010)

32. K.B. Narayanan, N. Sakthivel, Green synthesis of biogenic metal nanoparticles by terrestrial and aquatic phototrophic and heterotrophic eukaryotes and biocompatible agents. Adv. Colloid Interface Sci. **169**, 59–79 (2011)

33. Y. Park, Y.N. Hong, A. Weyers, Y.S. Kim, R.J. Linhardt, Polysaccharides and phytochemicals: a natural reservoir for the green synthesis of gold and silver nanoparticles. IET Nanobiotechnol. **5**, 69–78 (2011)

34. X. Huang, H. Wu, S. Pu, W. Zhang, X. Liao, B. Shi, One-step room-temperature synthesis of Au@ Pd core–shell nanoparticles with tunable structure using plant tannin as reductant and stabilizer. Green Chem. **13**, 950–957 (2011)

35. Q. Li, S. Mahendra, D.Y. Lyon, L. Brunet, M.V. Liga, D. Li, P.J.J. Alvarez, Antimicrobial nanomaterials for water disinfection and microbial control: potential applications and implications. Water Res. **42**, 4591–4602 (2008)

36. S.S. Shankar, A. Ahmad, R. Pasricha, M. Sastry, Bioreduction of chloroaurate ions by geranium leaves and its endophytic fungus yields gold nanoparticles of different shapes. J. Mater. Chem. **13**, 1822–1826 (2003)

37. S.K. Sivaraman, I. Elango, S. Kumar, V. Santhanam, A green protocol for room temperature synthesis of silver nanoparticles in seconds. Curr. Sci. **97**, 7 (2009)

38. A. Zyoud, A. Zu, M.H.S. Helal, D. Park, G. Campet, H.S. Hilal, Optimizing photo-mineralization of aqueous methyl orange by nano-ZnO catalyst under simulated natural conditions. J. Environ. Health Sci. Eng. **13**, 1–10 (2015). https://doi.org/10.1186/s40201-015-0204-0

39. C.M.V. Lakshmi, R. Ramith, R. Udayabhanu, Facile microwave-assisted green synthesis of ZnO nanoparticles: application to photodegradation, antibacterial and antioxidant. J. Mater. Sci. Mater. Electron. **31**, 1004–1021 (2020). https://doi.org/10.1007/s10854-019-02612-2

40. Y. Guo, X. Fu, R. Liu, M. Chu, W. Tian, Efficient green photocatalyst of Ag/ZnO nanoparticles for methylene blue

photodegradation. J. Mater. Sci. Mater. Electron. **33**, 2716–2728 (2022)